

Article

Fundamental Study on Electric Arc Furnace Steelmaking with Submerged Carbon Powder Injection with CO₂-O₂ Mixed Gas

Jianjun Li ^{1,2}, Guangsheng Wei ^{3,4,*} and Chengjin Han ³

¹ National Engineering Research Center of Continuous Casting Technology, China Iron & Steel Research Institute Group, Beijing 100081, China

² Metallurgical Corporation of China Co., Ltd., Beijing 100028, China

³ School of Metallurgical and Ecological Engineering, University of Science and Technology Beijing, Beijing 100083, China

⁴ Liaoning Academy of Materials, Shenyang 110000, China

* Correspondence: weiguangsheng@ustb.edu.cn

Abstract: The technology of submerged carbon powder injection with CO₂ and O₂ mixed gas (SCPI-COMG) is a new type of powder injection technology. It can increase the molten bath carbon content and improve the molten steel quality by injecting carbon powder directly into the molten steel with CO₂ and O₂ mixed gas. To optimize the process parameters of this novel technology, the mechanism of this technology and the effect of SCPI-COMG on EAF steelmaking were investigated in this study. Based on an induction furnace experiment, the effects of molten bath carburization and fluid flow on the scrap melting were analyzed. A mathematical model of the axis of gas jets in liquid steel was built to analyze the impact behaviors of gas jets in liquid steel. Based on the results of this theoretical model, for a gas jet in liquid steel, with $\alpha \geq 20^\circ$, the horizontal inject distance decreases with α increasing and with $0^\circ \leq \alpha \leq 20^\circ$, the horizontal inject distance increases with α increasing. Finally, based on the newly built materials and energy balance model of EAF steelmaking with SCPI-COMG, the influences of the gas-solid parameters on the EAF steelmaking technical indexes were also analyzed. is very useful for optimizing the process parameters of EAF steelmaking with SCPI-COMG. The results of this study are very useful to optimize the process parameters of EAF steelmaking with SCPI-COMG of Gas Jet in Liquid Steel.



Citation: Li, J.; Wei, G.; Han, C. Fundamental Study on Electric Arc Furnace Steelmaking with Submerged Carbon Powder Injection with CO₂-O₂ Mixed Gas. *Metals* **2023**, *13*, 1602. <https://doi.org/10.3390/met13091602>

Academic Editor: Henrik Saxen

Received: 24 July 2023

Revised: 23 August 2023

Accepted: 11 September 2023

Published: 15 September 2023



Copyright: © 2023 by the authors. Licensee MDPI, Basel, Switzerland. This article is an open access article distributed under the terms and conditions of the Creative Commons Attribution (CC BY) license (<https://creativecommons.org/licenses/by/4.0/>).

Keywords: electric arc furnace steelmaking; submerged gas-solid jet; jet impact characteristics; material and energy modeling

1. Introduction

Nowadays, the electric arc furnace (EAF) steelmaking has been widely adopted for steel production on a worldwide scale and demonstrates great potential for development because EAF steelmaking can produce steel products flexibly with lower CO₂ emissions, which is very helpful in promoting recycling and utilization of scrap resources [1–3]. Recently in China, a large number of EAFs have been newly built, including ordinary AC EAF, Consteel EAF, EAF Quantum and so on. It can be predicted that EAF steelmaking will play a more and more important role in steelmaking and more and more steel grades will be produced by the EAF steelmaking process [4–6]. Therefore, the control and promotion of the quality of molten steel will be of great importance for EAF steelmaking.

Compared with converter steelmaking, high-quality steel production is always a key issue and challenge in EAF steelmaking because it is very difficult to produce molten steel with low phosphorous content, low nitrogen content and low oxygen content in an EAF [7–9]. In EAF steelmaking, the weakened molten bath reaction kinetics conditions make it hard to remove the phosphorus from the molten steel [10]. Due to the lack of a carbon source by scrap charging, the carbon and oxygen reaction is considerably insufficient in the molten bath, which leads to the lack of CO bubbles. As a result, metallurgical problems occur,

such as the great difficulty in nitrogen removal and the serious peroxidation of molten steel [11,12]. Generally, carbonaceous materials are charged into the EAF to increase the carbon content of the molten steel, such as pig iron and coke. However, pig iron is produced by blast furnaces and the process is of high energy consumption, which is bad for green steelmaking [13]. Coke would float up and burn on the surface of the molten bath during the smelting process and its utilization ratio is very low. Therefore, based on the powder injection technology, the technology of submerged carbon powder injection with CO_2 and O_2 mixed gas (SCPI-COMG) was proposed and developed, which injects carbon powder directly into the molten steel with CO_2 and O_2 mixed gas (shown in Figure 1) [14,15]. Firstly, the method of delivery of carbon powder directly into the molten steel significantly improves the carbon pick-up of the molten steel. Secondly, the gas flow rate of the submerged injection is about 300 to $600 \text{ Nm}^3/\text{h}$ and the stirring of the EAF molten bath can be noticeably enhanced. In industrial application research, the metallurgical effects have been improved significantly in EAF steelmaking with SCPI-COMG. Wei et al. [16] used water model experiments and numerical simulations performed to investigate the flow field characteristics in the EAF metal bath under combined blowing, considering two merged nodules and two oven wall oxygen lands. However, as a novel method, the mechanism of this technology and the effect of SCPI-COMG on EAF steelmaking process have not been clear, which is very useful to optimize the process parameters of EAF steelmaking with SCPI-COMG.

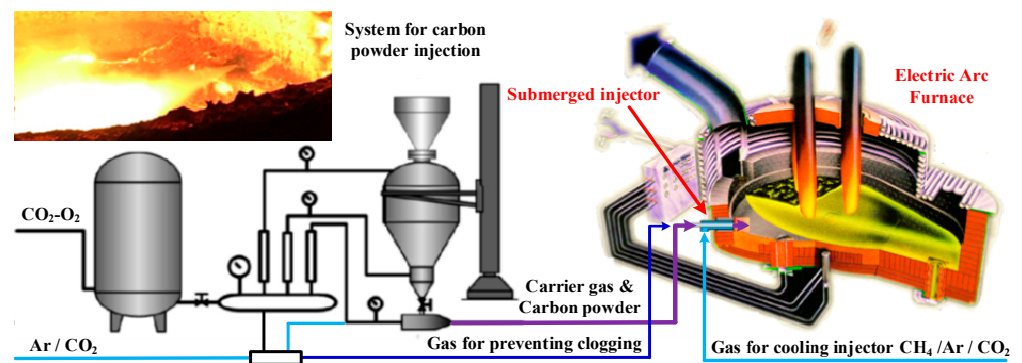


Figure 1. The system of submerged carbon powder injection with CO_2 - O_2 mixed gas in EAF.

In this study, some fundamental studies were carried out to understand and analyze the mechanism of EAF steelmaking with SCPI-COMG. An induction furnace experiment was carried out to investigate the mechanism of scrap melting by molten bath carburization and molten bath fluid flow. To analyze the impact behaviors of the gas jet in liquid steel, a mathematical model of the axis of the gas jet in liquid steel was built. The materials and energy balance model of EAF steelmaking with SCPI-COMG was built to study the influence of the gas-solid parameters on the EAF steelmaking technical indexes.

2. Mechanism for Improving Scrap Melting by Molten Bath Carburization

2.1. Experimental Platform

In order to study the mechanism for improving scrap melting by molten bath carburization with the SCPI-COMG technology, the experimental platform was built as Figure 2 shows, which includes a medium frequency induction furnace, a buffer vessel with N_2 cylinders, a fixing device, a Pt-Rh-Pt thermocouple, an infrared radiation thermometer and a computer. In this study, the diameter of the steel bar used for the experiment was 20 mm. The C content of the bar was about 0.45%. Melting baths with different C contents and different stirring intensities were used to study the influence of C content and melt flow on the melting of steel scrap. Physical changes such as weight changes and microstructural changes of the steel bar inserted in the bath were monitored and analyzed. The experimental program is shown in Table 1.

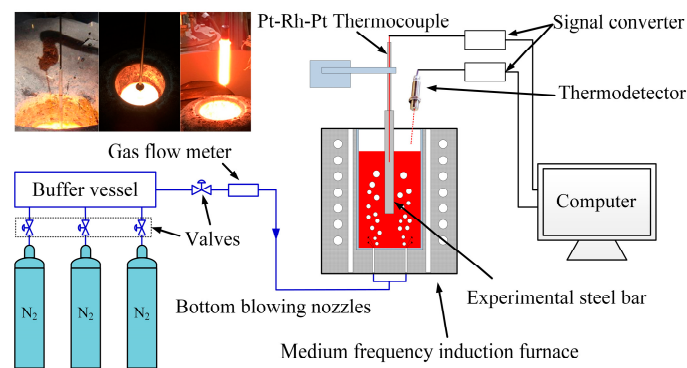


Figure 2. Experimental platform for scrap melting analysis.

Table 1. The composition of molten bath with different C content.

Label	w (C)%	w (Si)%	w (Mn)%	w (P)%	w (S)%	Gas Flow Rate
High carbon content	4.030	0.640	0.310	0.036	0.015	3.0 L/min
High carbon content	3.010	0.620	0.320	0.037	0.016	3.0 L/min
High carbon content	2.100	0.630	0.330	0.037	0.015	3.0 L/min
Weaker stirring	3.010	0.620	0.320	0.037	0.016	3.0 L/min
Medium stirring	3.030	0.580	0.360	0.033	0.014	5.0 L/min
Stronger stirring	2.980	0.610	0.350	0.034	0.017	7.0 L/min

2.2. Analysis of Experimental Results

The melting process of scrap consists of three stages: the iron coagulating stage, the carburizing and melting stage, and the full boiling stage [17–19]. The iron coagulating stage occurs initially after the steel bar's immersion into the molten bath. The large temperature gradient between the steel bar and the molten pool causes some of the molten metal to freeze quickly on the surface of the steel bar. The carburizing and melting stage is the controlling unit of the melting of scrap in EAF steelmaking. During this stage, carbon from the molten metal penetrates the surface of the scrap, thus accelerating the scrap melting process. In the full boiling stage, the temperature of the molten bath is larger than the steel melting point and the scrap melting rate is very faster.

Actually, the carburization process of the carburizing and melting stage is the main link. Based on the iron-carbon phase diagram, the iron-carbon alloy melting point is decreased by 78.5 °C with a 1.0% increase in the C content of iron-carbon alloy [20,21]. Thus, when the molten bath temperature is higher than the melting point of the carburized layer, the molten metal flowing around it will melt the carburized layer.

Figure 3a,b show the steel bar weight change with different molten bath carbon content and different molten bath stirring intensity, respectively. As shown in Figure 3a, the lower the C content in the melt bath, the heavier the steel bar weight. The mass melting rates for the low, medium and high C content baths were 1.19 g/s, 0.96 g/s and 0.79 g/s, respectively, for 0 s to 30 s. The mass melting rates were 2.98 g/s, 2.66 g/s and 2.14 g/s for low, medium and high carbon content in the melt pool from 40 s to 55 s, respectively. In addition to this, this phenomenon is also observed in other time periods. In Figure 3b, the weaker the stirring of the bath, the higher the weight of the bars. The mass melting rate is 1.06 g/s, 0.1.05 g/s and 0.96 g/s for strong, medium and weak bath agitation from 0 s to 30 s. The mass melting rate is 3.02 g/s, 2.87 g/s and 2.66 g/s for bottom-blowing gas flow rates of 7.0 L/min, 5.0 L/min and 3.0 L/min from 40 s to 55 s, respectively. The same phenomenon also can be found in other time ranges.

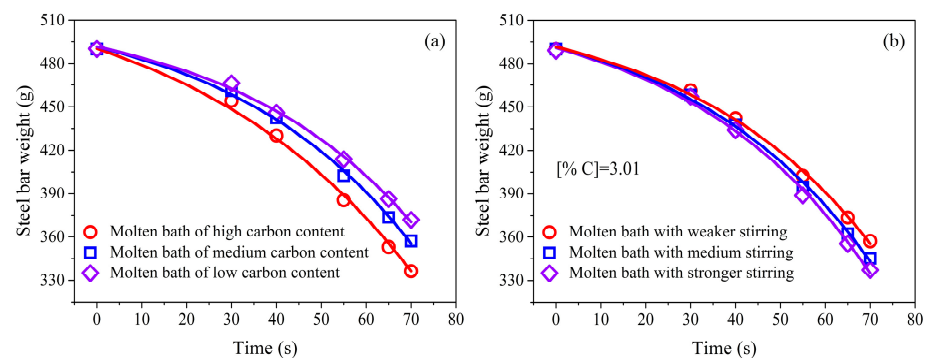


Figure 3. Weight change of the steel bar in molten bath with different C content and different stirring intensity: (a) different C content; (b) different stirring intensity.

According to the experimental results, the carbon content of the melt bath and the intensity of the melt bath stirring have a significant effect on the melting of the scrap. The lower the melt bath carbon content, the slower the melt bath stirring, then the slower the scrap melting rate. The smaller the carbon concentration gradient, the slower the carburization reaction speed. The lower intensity of bath stirring results in a lower convective heat transfer coefficient, which reduces the heat transfer from molten metal to scrap. For EAF steelmaking with SCPI-COMG, the molten bath carbon content can be effectively increased by the direct carbon injection into the molten steel of high temperature and the molten bath stirring can be noticeably enhanced by submerged injection with CO_2 and O_2 mixed gas, which is of large gas flow rate. Therefore, the SCPI-COMG technology can shorten tap-to-tap time by accelerating the smelting of scrap. What is more, the quality of molten steel also can be improved by increasing the melting down carbon content. The higher the carbon content of the molten bath, the more CO bubbles in the molten bath and the better the reaction kinetics conditions. Hence, the dephosphorization efficiency can be improved and the peroxidation of molten steel can be reduced. What is more, more CO bubbles can capture more nitrogen from the molten steel.

3. Impact Behaviors of Gas Jet in Liquid Steel

In SCPI-COMG, the carbon powder injection is a dilute phase convey, and therefore, the gas jet plays a main role in impacting and stirring the molten bath. As Figure 4 shows, in order to investigate the impact behaviors of gas jets in liquid steel in EAF steelmaking, the geometric model of gas jets in liquid steel was built on the basis of the water model experiment results and relative research [22]. In this study, a mathematical model was built to predict the formula of the axis of the gas jet in liquid steel.

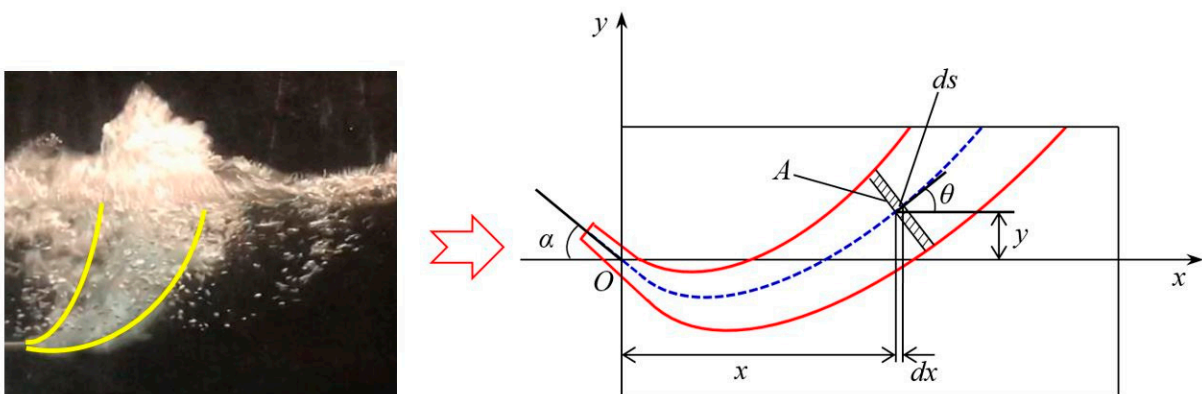


Figure 4. Geometric model of the gas jet in liquid steel [23].

3.1. Assumptions

- (1) The gas jet in liquid steel is regarded as a stable and incompressible fluid.
- (2) There are only mass and momentum exchanges between the jet and the surrounding liquid.
- (3) The momentum of the gas jet in liquid steel is conserved in the horizontal direction.
- (4) The transient variation of the momentum of the gas jet in liquid steel in the vertical direction is equal to the buoyancy of the jet.

3.2. Theoretical Modeling

As Figure 4 [23] shows, a microelement at the horizontal distance x ($h - x$) and $x + dx$ was regarded as a computing primitive, which is vertical to the jet axis. Based on the law of conservation of mass, the following equation can be obtained.

$$C_g \rho_g A v = \rho_g A_0 v_0 \quad (1)$$

where A and A_0 are the jet sectional area at $h - x$ and the exit of the injector, respectively; v and v_0 are the jet velocity at $h - x$ and the exit of the injector, respectively; ρ_g is the gas velocity; due to the entrainment of the jet, the gas jet in liquid steel in the molten bath would become gas-liquid jet, and therefore, $C_g + C_L = 1$, C_g and C_L are the gas and liquid volume fraction in the jet at $h - x$, respectively.

The momentum of the gas jet in liquid steel is conserved in the horizontal direction. The following equation can be obtained.

$$\rho_m A v^2 \cos \theta = \rho_g A_0 v_0^2 \cos \alpha \quad (2)$$

where α is the angle between the axis of the injector and the horizontal direction; ρ_m is the gas-liquid jet density calculated from ρ_g and ρ_L ; θ is the angle between the jet axis and the horizontal direction.

The calculation formula is as follows.

$$\rho_m = C_g \rho_g + C_L \rho_L \quad (3)$$

As a result, the following equation can be obtained by combining Equations (1)–(3).

$$\frac{\rho_L - \rho_m}{\rho_m} = \frac{\rho_L - \rho_g}{\rho_g} \frac{v_x}{v_0 \cos \theta} \quad (4)$$

The momentum of the gas jet in liquid steel is conserved in the vertical direction. The following equation can be obtained.

$$d(mv_y) = F_b \quad (5)$$

where m is the mass of the computing primitive at $h - x$; v_y is the velocity component in y direction at $h - x$ and F_b is the buoyancy of the the computing primitive at $h - x$.

$$F_b = (\rho_L - \rho_m) g A ds \quad (6)$$

where ds is the axis length of the computing primitive at $h - x$ and it can be calculated by the following equation.

$$ds = \frac{dx}{\cos \alpha} \quad (7)$$

As a result, the following equation can be obtained by combining Equations (5)–(7).

$$\frac{dv_y}{dx} + v_y \frac{d(\ln m)}{dx} - \frac{(\rho_L - \rho_m)g}{\rho_m v \cos \alpha} = 0 \quad (8)$$

Then, the following equation can be obtained by combining Equations (4) and (8).

$$\frac{dv_y}{dx} + v_y \frac{d(\ln m)}{dx} - \frac{(\rho_L - \rho_g)}{\rho_g} \frac{g}{v_0 \cos \theta} = 0 \quad (9)$$

For the convenience of analysis, we have assumed the following dimensionless variables.

$$x_r = \frac{x}{d_0}, y_r = \frac{y}{d_0}, v_{xr} = \frac{v_x}{v_0}, v_{yr} = \frac{v_y}{v_0}$$

$$v_r = \frac{v}{v_0}, m_r = \frac{m}{\rho_g A_0 v_0}, Fr' = \frac{\rho_g v_0^2}{(\rho_L - \rho_g) g d_0}$$

where d_0 is the injector exit diameter and Fr' is the modified Froude. Hence, the following equations can be obtained.

$$\frac{dv_{yr}}{dx_r} + v_{yr} \frac{d(\ln m_r)}{dx_r} - \frac{1}{Fr' \cos \theta} = 0 \quad (10)$$

$$m_r = \frac{\cos \theta}{v_{xr}} \quad (11)$$

Based on Equations (10) and (11), the following Equation (12) can be obtained by mathematical transformations.

$$\frac{d^2 y_r}{dx_r^2} = \frac{1}{Fr' v_{xr} \cos \theta} \quad (12)$$

According to the previous report, the following equation can be adopted in this study.

$$v_{xr} = \frac{K \cos \alpha}{x_r + K} \quad (13)$$

where K is a constant.

Therefore, the following equation can be obtained by combining Equations (12) and (13).

$$\frac{d^2 y_r}{dx_r^2} = \frac{1}{K Fr' \cos^2 \theta} \frac{x_r + K}{x_r + K} \quad (14)$$

According to the boundary conditions of Equation (14), the mathematical model to depict the formula of the axis of the gas jet in liquid steel can be obtained.

$$y_r = \frac{1}{K Fr' \cos^2 \theta} \left[\frac{1}{6} x_r^3 + \frac{K}{2} x_r^2 + \frac{\sin 2\alpha}{2} K Fr' x_r \right] \quad (15)$$

Therefore, for a gas jet in liquid steel, the axis of the jet in the molten steel can be calculated by Equation (15) on the basis of the installed angle, the submerged depth and the gas flow rate. For model validation, the theoretical model was also verified by the water model experiment (Figure 5).

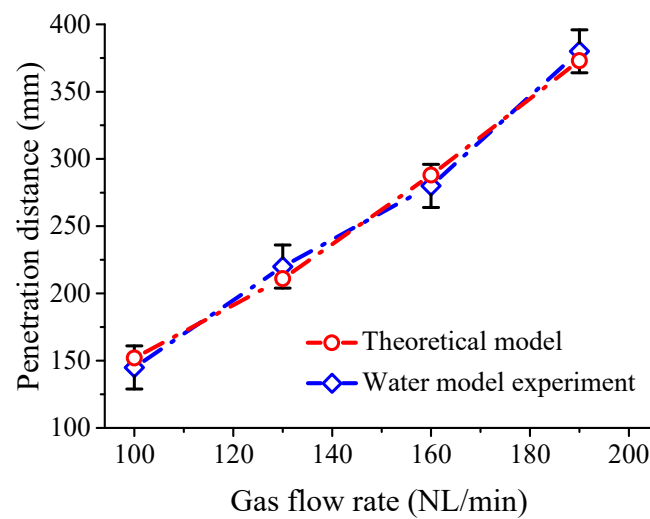


Figure 5. Comparison of the horizontal inject distance between the theoretical model values and the water model experiment results.

3.3. Analysis of Impact Behaviors of Gas Jet in Liquid Steel

In EAF steelmaking with SCPI-COMG, the injector is under the molten steel level in the range of 500 to 700 mm, which depends on the furnace profile and the diameter of the submerged injector exit is about 12 mm. Therefore, the dimensionless quantity of the submerged depth y_r is in the range of 40 to 60 approximately.

According to the experimental results, when the vertical impact depth reaches 700 mm, the maximum horizontal impact distance does not exceed 600 mm, which is much smaller than the actual diameter of the electric arc furnace melt pool. Therefore, the actual melt pool diameter will not affect the penetration depth of the jet.

Figure 6a [23] shows the axis trajectory of the gas jet in liquid steel with different installed angles. It can be found that with $0^\circ \leq \alpha \leq 20^\circ$, the horizontal inject distance increases with α increasing. The change trend is more obvious in the range of 0° to 10° . When α is larger than 20° , the horizontal inject distance decreases with α increasing. Hence, in industrial applications, the installed angle is about 10° . Certainly, the effect of the installed angle on the erosion of the refractory was also taken into account.

Figure 6b [23] shows the axis trajectory of the gas jet in liquid steel with different gas flow rates. It can be found that the inject distance increases with the gas flow rate increasing. With the same installed angle and the same injector exit diameter, the jet velocity at the exit of the injector could be increased by the larger gas flow rate. Therefore, both the horizontal and the vertical inject distance of the submerged are larger.

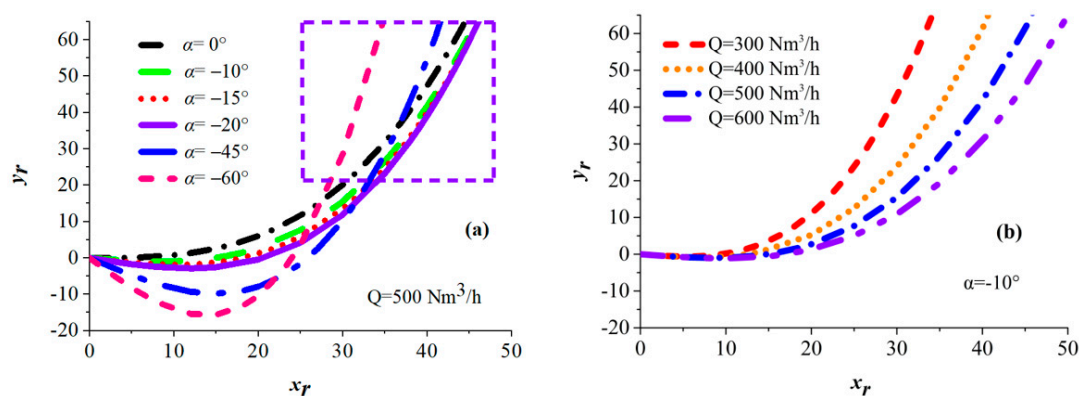


Figure 6. Axis trajectory of gas jet in liquid steel [23]. (a) Different installed angles with $Q = 500 \text{ Nm}^3/\text{h}$. (b) Different gas flow rates with $\alpha = -10^\circ$.

4. Influence of the Gas-Solid Parameters on the EAF Steelmaking Process

Based on the previous studies [24–27], the materials and energy balance model of EAF steelmaking with SCPI-COMG were built by combining the material balance, the energy balance and the chemical equilibrium (shown in Figure 7). These newly built models were tested in the case of a commercial 50-ton EAF with SCPI-COMG. The results of the theoretical calculation were in accord with the results of the industrial production (listed in Table 2), which could demonstrate that the materials and energy balance model was reasonable. In this study, these two models were employed to investigate the effect of the gas-solid parameters on the key technical parameters of EAF steelmaking.

Table 2. Comparison between the measured averaged values and the calculated averaged values of theoretical model.

Label		Carbon Powder Consumption (kg/t)	Power Consumption (kWh/t)	O ₂ Consumption (Nm ³ /t)
001	Calculated	12.0	380.9	27.7
	Measured	11.7	385.5	28.3
002	Calculated	16.0	369.1	33.1
	Measured	16.3	365.3	34.2
003	Calculated	20.0	358.5	36.3
	Measured	20.1	356.2	35.2
004	Calculated	23.0	354.7	39.5
	Measured	22.7	357.6	42.6
005	Calculated	28.0	350.8	44.9
	Measured	27.6	350.2	43.6
006	Calculated	32.0	348.3	49.2
	Measured	32.3	343.2	47.3

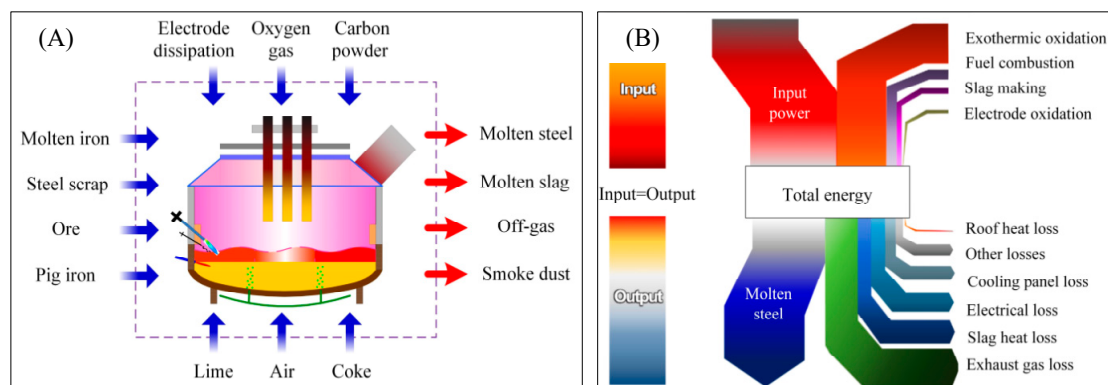


Figure 7. The materials and energy balance system model of EAF steelmaking; (A) materials balance system model, (B) energy balance system model.

4.1. Variation Tendency of the Molten Slag and the Off-Gas Volume

Figure 8 shows the effect of the carbon powder quantity on the molten slag in EAF steelmaking with SCPI-COMG. The quantity of the molten slag increases with the carbon powder quantity increasing. The quantity of the molten slag is 82.33 kg/t when the carbon powder quantity is 10 kg/t and that increases to 89.54 kg/t when the carbon powder quantity is 40 kg/t. The main reason is that the ash content in the carbon powder is about 12.4% and almost all of the ash is removed into the molten slag during the steelmaking process. In addition, after the increase in ash content, in order to ensure the alkalinity of the slag, lime and other slag-making materials need to be added to the slag, resulting in an increase in the remaining slag amount.

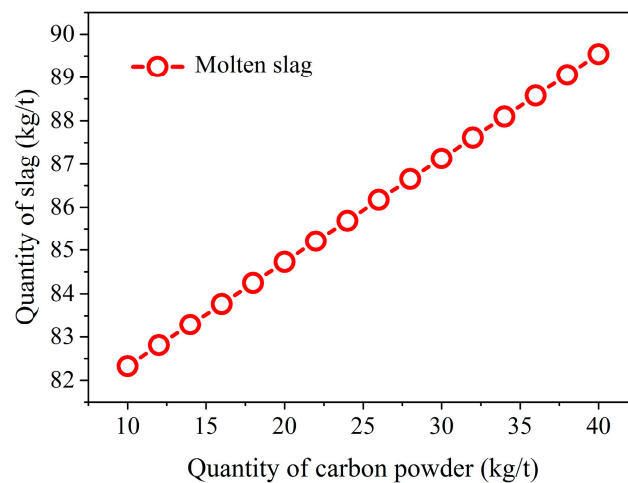


Figure 8. The relationship between the quantity of slag and the quantity of carbon powder.

As for the smelting off-gas, the addition of carbon powder and CO_2 influences the off-gas volume. With the carbon powder quantity increasing, the volume of the off-gas increases noticeably (shown in Figure 9). When the carbon powder quantity changed from 10 kg/t to 40 kg/t, the total volume of off-gas increased from $58.87 \text{ Nm}^3/\text{t}$ to $147.50 \text{ Nm}^3/\text{h}$, the volume of CO_2 changed from $22.98 \text{ Nm}^3/\text{t}$ to $61.54 \text{ Nm}^3/\text{t}$ and the volume of CO changes from $10.47 \text{ Nm}^3/\text{t}$ to $28.31 \text{ Nm}^3/\text{t}$. It can be found that the volume of CO_2 increased by a large margin. With the assumed CO post-combustion ratio, a large amount of CO_2 was formed due to the CO combustion and meanwhile, the powder carrier gas is also a main source of CO_2 . The volume and composition change law of the off-gas in EAF steelmaking with SCPI-COMG can offer the reference basis data to optimize the cooperative operation between the smelting system and the dust-removal system in EAF steelmaking.

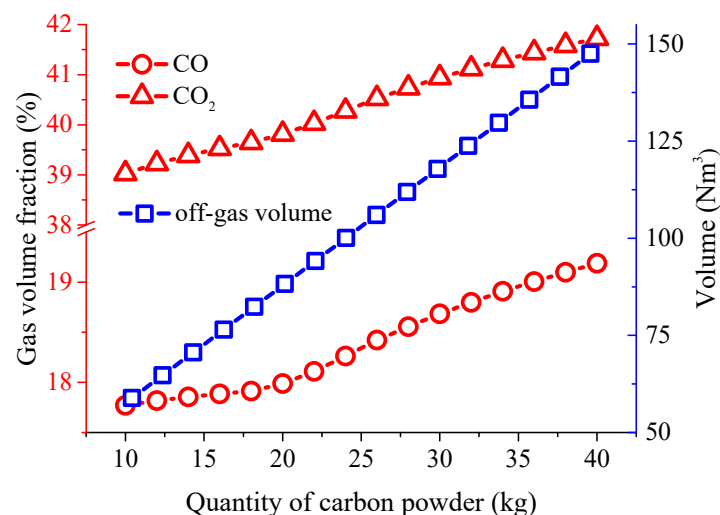


Figure 9. The relationship between the power consumption and the off-gas volume and composition.

4.2. Variation Tendency of the Power Consumption

Based on the above analysis, the SCPI-COMG technology can accelerate the melting process of scrap by enhancing the carburization of molten steel. Furthermore, a great deal of heat generated by the carbon and oxygen reaction can also accelerate the smelting rhythm and reduce power consumption. Figure 10 shows the variation tendency of the power consumption with the quantity of carbon powder in EAF steelmaking with SCPI-COMG. On one hand, it can be found that the power consumption decreases with the quantity of carbon powder increasing. Based on the calculation results, a 1 kg/t increase

in the quantity of carbon injected into the molten steel by SCPI-COMG would decrease the power consumption by about 3 to 4 kWh/t. On the other hand, the decrease of power consumption is gradually reduced with the quantity of carbon powder increasing. The average decrease speed of the power consumption per ton of steel is about 3.6 kWh per kg carbon powder when the quantity of carbon powder is less than 20 kg/t and that would become 0.7 kWh per kg carbon powder when the quantity of carbon powder in the range of 30 to 40 kg/t. That is, the effective utilization efficiency of carbon powder decreases as the quantity of carbon powder increases. With a large injection rate of the carbon powder, the instantaneous ability to dissolve carbon powder in the molten bath is limited and hence, a part of the carbon powder escapes directly from the molten steel into the furnace tank before they are captured by the molten steel. Furthermore, the more carbon powder is injected, the more carbon escapes into the furnace tank. Hence, the effective utilization efficiency of carbon powder decreases with more carbon powder. Therefore, the injection parameters of the SCPI-COMG technology should be adjusted and optimized according to the actual smelting conditions during the EAF steelmaking process, such as the burden design, the smelting stage and so on.

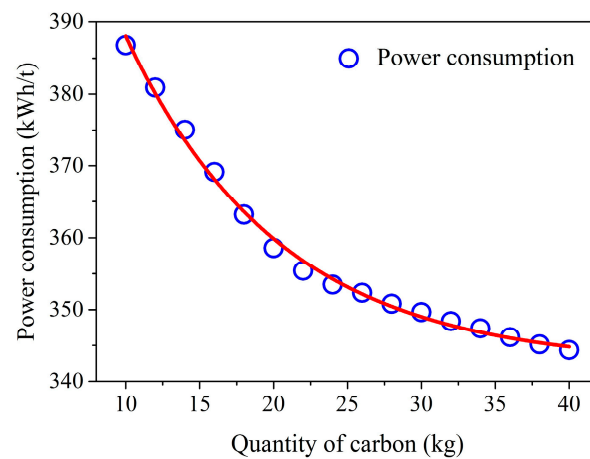


Figure 10. The relationship between the power consumption and the quantity of carbon powder.

4.3. Effective Utilization and Burning Loss of Carbon Powder

In this paper, the burning loss of carbon powder is defined as the carbon powder that reacts directly with CO_2 and O_2 and this part of carbon powder is not captured by the molten steel during the EAF steelmaking process with SCPI-COMG. Figure 11 shows the relationship between the carbon powder burning loss and the quantity of carbon powder. It can be found that when the quantity of carbon powder is less than 20 kg/t; the burning loss rate of carbon powder with O_2 is almost invariable and the burning loss rate of carbon powder with CO_2 decreases gradually with the increasing quantity of carbon powder. In this range, with the carbon powder quantity increasing, the proportion of carbon powder melting into the molten steel decreases and correspondingly, the power consumption decreases. When the quantity of carbon powder is in the range of 20 kg/t to 40 kg/t, the burning loss rate of carbon powder with O_2 increases gradually and the burning loss rate of carbon powder with CO_2 decreases slightly with the quantity of carbon powder increasing. It demonstrates that with the quantity of carbon powder increasing, more and more carbon powder ran out from the molten bath into the furnace tank without carburization and this part of carbon powder was burnt by O_2 in the furnace tank directly. However, compared with the carbon and oxygen reaction in the molten steel during the steelmaking process, heat generated by the combustion reaction between carbon powder and O_2 in the furnace tank can be utilized by the molten bath. Therefore, the speed of the power consumption is gradually reduced.

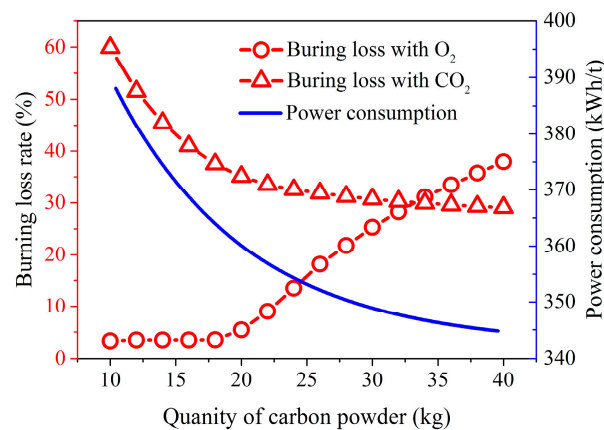


Figure 11. The relationship between the carbon powder burning loss and the quantity of carbon powder.

Assuming the injection mass ratio $\text{CO}_2:\text{O}_2 = 5.5$; CO_2 utilization rate of 80%; 98% O_2 utilization rate; CO_2 purity is 99%. The burning reaction between carbon powder and O_2 and CO_2 is as follows:



Based on the industrial application research, the melting down of carbon contents with different carbon powder quantities was measured and the corresponding effective utilization ratio of carbon powder melting into the molten steel was also calculated (shown in Figures 12 and 13). When the quantity of carbon powder is less than 20 kg/t, the melting down carbon content of the EAF molten bath is proportional to the quantity of carbon powder and the effective utilization ratio of carbon powder increases stably. When the quantity of carbon powder is in the range of 20 kg/t to 40 kg/t, it can be found that with the quantity of carbon powder increasing, the melting down carbon content increases more and more slowly and the effective utilization ratio of carbon powder decreases correspondingly.

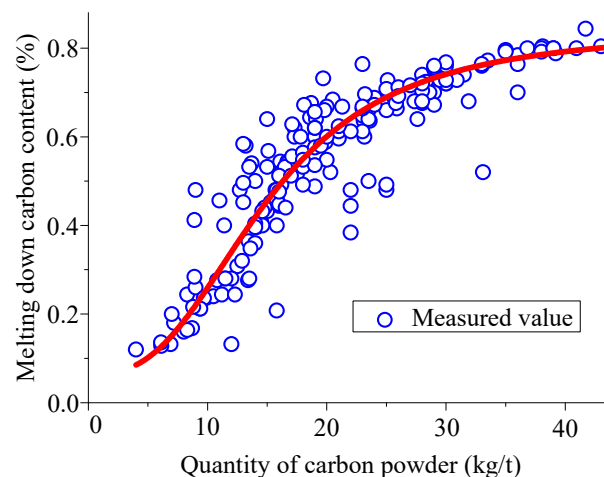


Figure 12. The melting down carbon content with different carbon powder quantity in the industrial application.

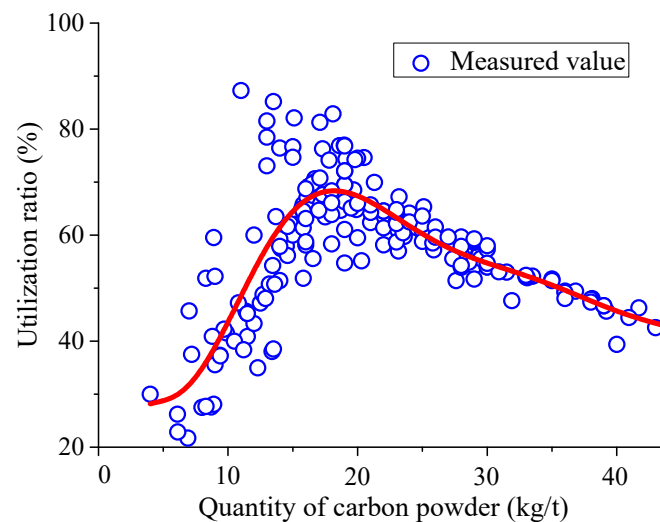


Figure 13. The rate of carbon powder melting into the molten steel with different carbon powder quantity in the industrial application.

4.4. Effect of CO Post-Combustion on the Power Consumption

In EAF steelmaking, a large amount of CO is generated during the smelting process and these CO gas contains massive chemical latent heat, which is useful to reduce the smelting energy consumption [28,29]. Actually, it is significant to enhance the CO post-combustion and improve the energy utilization rate of CO post-combustion. Figure 14a,b show the relationship between the power consumption and the CO post-combustion ratio and the relationship between the power consumption and the energy utilization rate of CO post-combustion, respectively. In Figure 14a, the energy utilization rate of CO post-combustion is assumed as 42%. With the CO post-combustion ratio increasing, the power consumption decreases. A 1% increase in the CO post-combustion ratio would decrease the power consumption by 0.76 kWh/t. In Figure 14b, the CO post-combustion ratio is assumed as 55%. And with the energy utilization rate of CO post-combustion increasing, the power consumption decreases. A 1% increase in the energy utilization rate of CO post-combustion would decrease the power consumption by 1.6 kWh/t. In EAF steelmaking with SCPI-COMG, the quantity of carbon powder injected into the EAF steelmaking system is far more than that in traditional EAF steelmaking. Hence, the utilization and optimization of CO post-combustion is of greater importance. Generally, the CO post-combustion includes CO post-combustion in foaming slag and CO post-combustion in free space [30,31]. With CO post-combustion in free space, the heat generated by the reaction between O_2 and CO above the molten bath is transformed into the molten slag layer by radiation and convection and then the heat is transformed from the molten slag layer to molten steel. In this heat transfer process, the energy utilization rate is only about 20% to 40%. With CO post-combustion in foaming slag, the heat generated is directly transformed into molten steel from the molten slag layer, which improves the efficiency of energy utilization noticeably. Therefore, in EAF steelmaking with SCPI-COMG, it is very important to enhance the CO post-combustion, especially the CO post-combustion in foaming slag, to increase the energy utilization rate and reduce the power consumption.

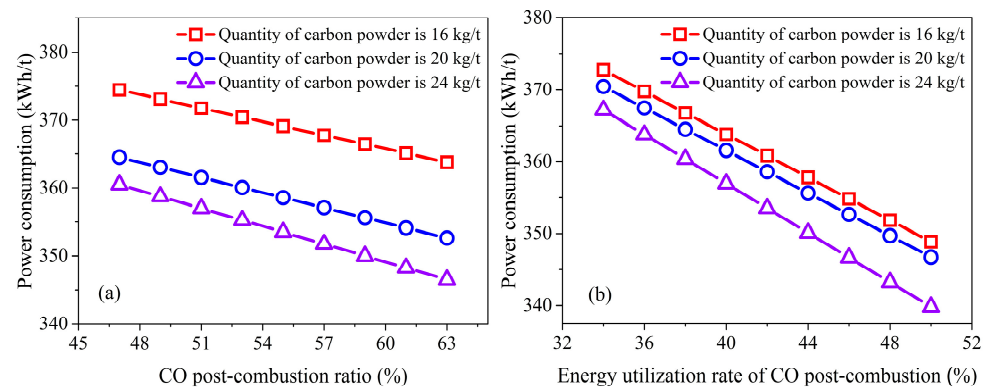


Figure 14. The relationship between the power consumption and the CO post-combustion parameters. (a) CO post-combustion ratio. (b) Energy utilization rate of CO post-combustion.

5. Conclusions

Some fundamental studies were carried out to understand the mechanism of EAF steelmaking with SCPI-COMG. An induction furnace experiment was carried out to investigate the mechanism of scrap melting by molten bath carburization and fluid flow. The mathematical model of the axis of the gas jet in liquid steel was built to analyze the impact characteristics of gas jet in liquid steel, and the materials balance model and energy balance model of EAF steelmaking with SCPI-COMG were built and tested to study the influence of the gas-solid parameters on the EAF steelmaking process.

In the EAF steelmaking process using the SCPI-COMG, the carbon content of the melt bath and the intensity of the melt bath stirring have a significant effect on the melting of the scrap. The lower the melt bath carbon content, the slower the melt bath stirring, then the slower the scrap melting rate. The smaller the carbon concentration gradient, the slower the carburisation reaction speed. The lower intensity of bath stirring results in a lower convective heat transfer coefficient, which reduces the heat transfer from molten metal to scrap.

The mathematical model built to depict the formula of the axis of the gas jet in liquid steel can well predict the axis trajectory of the gas jet in liquid steel. Based on the results of this theoretical model, for a gas jet in liquid steel, with $\alpha \geq 20^\circ$, the horizontal penetration distance decreases with α increasing and with $0^\circ \leq \alpha \leq 20^\circ$, the horizontal penetration distance increases with α increasing. Especially in the range of 0° to 10° , the change trend is more obvious.

The materials and energy balance model of EAF steelmaking with SCPI-COMG was in accord with the industrial application. Based on the results of these two models, it can be found that with the carbon powder quantity increasing, the power consumption decreases, the quantity of the molten slag increases and the off-gas volume increases. When the quantity of carbon powder is more than 20 kg/t, the effective utilization efficiency of carbon powder decreases as the quantity of carbon powder increases. The CO post-combustion is useful to reduce the smelting energy consumption in EAF steelmaking. Hence, with SCPI-COMG, it is very important to enhance the CO post-combustion, especially the CO post-combustion in foaming slag, to increase the energy utilization rate and reduce the power consumption.

Author Contributions: The contributions of the authors are as follows: J.L.: Conceptualization, Methodology, Project administration, Writing—Original Draft. G.W.: Conceptualization, Methodology, Writing—Review and Editing, Supervision. C.H.: Writing—Review and Editing, Supervision, Software, Validation. All authors have read and agreed to the published version of the manuscript.

Funding: This research was funded by the National Nature Science Foundation of China (No. 52274313, No. 52293392, No. 52004023 and No. 52074024) and Key R&D Projects of Jiangxi Province 20214BBG74005.

Data Availability Statement: No new data were created or analyzed in this study. Data sharing is not applicable to this article.

Conflicts of Interest: The authors have no relevant financial or non-financial interests to disclose.

References

1. Lee, B.; Sohn, I. Review of Innovative Energy Savings Technology for the Electric Arc Furnace. *JOM* **2014**, *66*, 1581–1594. [[CrossRef](#)]
2. Kirschen, M.; Badr, K.; Pfeifer, H. Influence of direct reduced iron on the energy balance of the electric arc furnace in steel industry. *Energy* **2011**, *36*, 6146–6155. [[CrossRef](#)]
3. Kerimov, R.I.; Shakhov, S.I. Use of Metallized Raw Materials in Electric Furnace Steelmaking. *Metallurgist* **2020**, *64*, 128–135. [[CrossRef](#)]
4. Toulouevski, Y.N.; Zinurov, I.Y. *Innovation in Electric Arc Furnaces*; Springer: Berlin/Heidelberg, Germany, 2010; pp. 1–20.
5. Wei, G.; Zhu, R.; Dong, K.; Ma, G.; Cheng, T. Research and Analysis on the Physical and Chemical Properties of Molten Bath with Bottom-Blowing in EAF Steelmaking Process. *Metall. Mater. Trans. B* **2016**, *47*, 3066. [[CrossRef](#)]
6. Yang, Z.; Yang, L.; Cheng, T.; Chen, F.; Zheng, F.; Wang, S.; Guo, Y. Fluid Flow Characteristic of EAF Molten Steel with Different Bottom-Blowing Gas Flow Rate Distributions. *ISIJ Int.* **2020**, *60*, 1957–1967. [[CrossRef](#)]
7. Li, M.; Shao, L.; Li, Q.; Zou, Z. A Numerical Study on Blowing Characteristics of a Dynamic Free Oxygen Lance Converter for Hot Metal Dephosphorization Technology Using a Coupled VOF-SMM Method. *Metall. Mater. Trans. B* **2021**, *52*, 2026–2037. [[CrossRef](#)]
8. Dong, P.; Zheng, S.; Zhu, M. Numerical Study on Gas-Metal-Slag Interaction with Single-Flow Postcombustion Oxygen Lance in the Steelmaking Process of a Top-Blown Converter. *JOM* **2022**, *74*, 1509–1520. [[CrossRef](#)]
9. Zurutuza, I.; Isasti, N.; Detemple, E.; Schwinn, V.; Mohrbacher, H.; Uranga, P. Effect of dynamic recrystallization on microstructural evolution in B steels microalloyed with Nb and/or Mo. *Materials* **2022**, *15*, 1424. [[CrossRef](#)]
10. Dong, K.; Zhu, R.; Liu, W.J. Bottom-Blown Stirring Technology Application in Consteel EAF. *Adv. Mater. Res.* **2012**, *361–363*, 639–643. [[CrossRef](#)]
11. Singh, M.K.; Keshari, K.K.; Prasad, A.; Das, A. Effect of Steel Making Parameters on Nitrogen Level in Steel. *Process. Charact. Mater.* **2021**, *13*, 63–73. [[CrossRef](#)]
12. Harashinia, K.; Mizoguchi, S.; Kajioka, H. Kinetics of Nitrogen Desorption from Low Nitrogen Liquid Iron by Blowing Ar and Reducing Gas Mixture or by Top Injection of Iron Ore Powder under Reduced Pressure. *Tetsu-to-Hagane* **1988**, *74*, 441–448. [[CrossRef](#)]
13. Lee, M.; Trotter, D.; Mazzei, O. The production of low phosphorus and nitrogen steels in an EAF using HBI. *Scand. J. Met.* **2001**, *30*, 286–291. [[CrossRef](#)]
14. Wei, G.; Zhu, R.; Wu, X.; Dong, K.; Yang, L.; Liu, R. Technological Innovations of Carbon Dioxide Injection in EAF-LF Steelmaking. *JOM* **2018**, *70*, 969–976. [[CrossRef](#)]
15. Zhu, R.; Wei, G.; Tang, T. Technologies of purification production in electric arc furnace steelmaking processes. *Steelmaking* **2018**, *34*, 10.
16. Wei, G.; Zhu, R.; Yang, S.; Wu, X.; Dong, K. Simulation and application of submerged CO₂-O₂ injection in EAF steelmaking: Combined blowing equipment arrangement and industrial application. *Ironmak. Steelmak.* **2021**, *48*, 703–711. [[CrossRef](#)]
17. Liu, M.; Ma, G.; Zhang, X.; Zheng, D. Numerical simulation on the melting kinetics of steel scrap in iron-carbon bath. *Case Stud. Therm. Eng.* **2022**, *34*, 101995. [[CrossRef](#)]
18. Wright, J.K. Steel dissolution in quiescent and gas stirred Fe/C melts. *Metall. Mater. Trans. B* **1989**, *20*, 363–374. [[CrossRef](#)]
19. Nomura, H.; Mori, K. The Rate of Dissolution Iron Into Liquid Fe-C Alloy. *Tetsu-to-Hagane* **1969**, *55*, 1134–1141. [[CrossRef](#)]
20. Matsuura, K.; Itoh, Y.; Narita, T. A Solid-Liquid Diffusion Couple Study of a Peritectic Reaction in Iron-Carbon System. *ISIJ Int.* **1993**, *33*, 583–587. [[CrossRef](#)]
21. Kim, Y.U.; Pehlke, R.D. Mass Transfer During Dissolution of a Solid Into Liquid in the Iron-Carbon System. *Metall. Trans.* **1974**, *5*, 2527–2532. [[CrossRef](#)]
22. Gulawani, S.S.; Deshpande, S.S.; Joshi, J.B.; Shah, M.S.; Prasad, C.S.R.; Shukla, D.S. Submerged Gas Jet into a Liquid Bath: A Review. *Ind. Eng. Chem. Res.* **2007**, *46*, 3188–3218. [[CrossRef](#)]
23. Wei, G.; Zhu, R.; Tang, T.; Dong, K.; Wu, X. Study on the Impact Characteristics of Submerged CO₂ and O₂ Mixed Injection (S-COMI) in EAF Steelmaking. *Metall. Mater. Trans. B* **2019**, *2*, 50. [[CrossRef](#)]
24. Opitz, F.; Treffinger, P.; Wöllenstein, J. Modeling of Radiative Heat Transfer in an Electric Arc Furnace. *Met. Mater. Trans. B* **2017**, *48*, 3301–3315. [[CrossRef](#)]
25. Logar, V.; Dovžan, D.; Škrjanc, I. Modeling and Validation of an Electric Arc Furnace: Part 1, Heat and Mass Transfer. *ISIJ Int.* **2012**, *52*, 402–412. [[CrossRef](#)]
26. Fathi, A.; Saboohi, Y.; Škrjanc, I.; Logar, V. Comprehensive Electric Arc Furnace Model for Simulation Purposes and Model-Based Control. *Steel Res. Int.* **2017**, *88*, 1600083. [[CrossRef](#)]
27. Odenthal, H.-J.; Kemminger, A.; Krause, F.; Sankowski, L.; Uebber, N.; Vogl, N. Review on Modeling and Simulation of the Electric Arc Furnace (EAF). *Steel Res. Int.* **2018**, *89*, 1700098. [[CrossRef](#)]
28. Irawan, A.; Kurniawan, T.; Alwan, H.; Muslim, Z.; Akhmal, H.; Firdaus, M.; Bindar, Y. An energy optimization study of the electric arc furnace from the steelmaking process with hot metal charging. *Heliyon* **2022**, *8*, 11. [[CrossRef](#)]
29. Krassnig, H.J.; Kleimt, B.; Voj, L. EAF post-combustion control by on-line laser-based off-gas measurement. *Arch. Metall. Mater.* **2008**, *53*, 455–462.

30. Ahmadi, A.; Bahiraei, M. Thermohydraulic performance optimization of cooling system of an electric arc furnace operated with nanofluid: A CFD study, *J. Clean. Prod.* **2021**, *310*, 127451. [[CrossRef](#)]
31. Yang, L.-Z.; Hu, H.; Yang, Z.-S.; Xue, B.-T.; Guo, Y.-F.; Wang, S. A review on bath fluid flow stirring technologies in EAF steelmaking. *J. Iron Steel Res. Int.* **2021**, *28*, 1341–1351. [[CrossRef](#)]

Disclaimer/Publisher’s Note: The statements, opinions and data contained in all publications are solely those of the individual author(s) and contributor(s) and not of MDPI and/or the editor(s). MDPI and/or the editor(s) disclaim responsibility for any injury to people or property resulting from any ideas, methods, instructions or products referred to in the content.